**Journal of Nuclear Medicine, published on September 13, 2018 as doi:10.2967/jnumed.118.216069**

# Title: Affibody-based PET imaging to guide EGFR-targeted cancer therapy in head and neck squamous cell cancer models

Thomas A. Burley[1], Chiara Da Pieve[1], Carlos D. Martins[1], Daniela M. Ciobota[1], Louis Allott[1], Wim J. G Oyen[1, 2], Kevin J. Harrington[1], Graham Smith[1], Gabriela Kramer-Marek[1*]

[1]Division of Radiotherapy and Imaging, The Institute of Cancer Research, 123 Old Brompton Road, London, SW7 3RP, UK

[2]The Royal Marsden NHS Foundation Trust, Department of Nuclear Medicine, Fulham Road, London, SW3 6JJ, UK

**Running title:** PET to guide EGFR-targeted therapy

**Disclosure statement:** No potential conflicts of interest relevant to this article exist.

**Corresponding author:**

*Gabriela Kramer-Marek

123 Old Brompton Road, London, SW7 3RP, UK

Phone: +44 208 722 4518

Email: Gabriela.Kramer-Marek@icr.ac.uk

**First author:**

Thomas A. Burley (PhD student)

123 Old Brompton Road, London, SW7 3RP, UK

Phone: +44 208 722 4412

Email: Tom.Burley@icr.ac.uk

**Word count**: 6148

**Financial support:** This research was supported in part by the by the Cancer Research UK-Cancer Imaging Centre (C1060/A16464) and EPSRC (EP/H046526/1). This report is independent research funded by the National Institute for Health Research. The views expressed in this publication are those of the authors and not necessarily those of the NHS, the National Institute for Health Research or the Department of Health.



## ABSTRACT

In head and neck squamous cell carcinoma (HNSCC), the human epidermal growth factor receptor 1 (EGFR) is the dominant signaling molecule among all members of the family. So far, cetuximab is the only approved anti-EGFR mAb used for the treatment of HNSCC, but despite the benefits of adding it to standard treatment regimens, attempts to define a predictive biomarker to stratify patients for cetuximab treatment have been unsuccessful. We hypothesized that imaging with EGFR-specific radioligands may facilitate non-invasive measurement of EGFR expression across the entire tumor burden and also allow for dynamic monitoring of cetuximab-mediated changes in receptor expression. **Methods:** EGFR-specific Affibody molecule ($Z_{EGFR:03115}$) was radiolabeled with zirconium-89 ($^{89}Zr$) and fluorine-18 ($^{18}F$). The radioligands were characterized *in vitro* and in mice bearing subcutaneous tumors with varying levels of EGFR expression. The protein dose for imaging studies was assessed by injecting $^{89}Zr$-DFO-$Z_{EGFR:03115}$ (2.4-3.6 MBq, 2 μg) either together with or 30 mins after increasing amounts of unlabeled $Z_{EGFR:03115}$ (1, 5, 10, 15 and 20 μg). PET images were acquired at 3, 24 and 48 h post-injection and the image quantification data were correlated with the biodistribution results. The EGFR expression and biodistribution of the tracer were assessed *ex vivo* by immunohistochemistry, Western blot and autoradiography. To downregulate the EGFR level, treatment with cetuximab was performed and $^{18}F$-AlF-NOTA-$Z_{EGFR:03115}$ (12 μg, 1.5-2 MBq/mouse) used to monitor receptor changes. **Results:** *In vivo* studies demonstrated that co-injecting 10 μg of non-labeled molecules with $^{89}Zr$-DFO-$Z_{EGFR:03115}$ allows for clear tumor visualization 3 h post-injection. The radioconjugate tumor accumulation was EGFR-specific and PET imaging data showed a clear differentiation between xenografts with varying EGFR expression levels. A

strong correlation was observed between PET analysis, *ex vivo* estimates of tracer concentration and receptor expression in tumor tissues. Additionally, $^{18}$F-AlF-NOTA-$Z_{EGFR:03115}$ could measure receptor downregulation in response to EGFR inhibition.

**Conclusion:** $Z_{EGFR03115}$-based radioconjugates can assess different levels of EGFR level *in vivo* and measure receptor expression changes in response to cetuximab, indicating a potential for assessment of adequate treatment dosing with anti-EGFR antibodies.

**Key Words**: Affibody molecules; EGFR, zirconium-89, fluorine-18, cancer imaging

## INTRODUCTION

Globally, head and neck squamous cell cancer (HNSCC) is the sixth most common cancer; its treatment consists of surgery and/or radiotherapy, with or without concurrent chemotherapy or targeted therapy (*1*). Disappointingly, patient survival has not markedly improved in recent decades and approximately 50% of patients with locally advanced disease will develop recurrence or metastases within 2 years. Such differences in outcome are largely driven by inter- and intra-patient heterogeneity in disease biology (*2*).

Of note, in HNSCC the human epidermal growth factor receptor 1 (EGFR) is the dominant member of the HER family (*3*). EGFR mRNA and receptor expression were found to be elevated in 92% and 38-47% of cases, respectively (*3,4*). Furthermore, this aberrant receptor expression and activity was positively correlated with poor patient prognosis and resistance to radiation therapy (*5*). These findings led to the development and widespread implementation of specific anti-EGFR inhibitors, including monoclonal antibodies (mAbs) targeting the extracellular domain of EGFR (e.g. cetuximab, panitumumab, zalutumumab) and small molecule tyrosine kinase inhibitors that target the intracellular domain (e.g. gefinitib, erlotinib) (*6*). So far, cetuximab is the only anti-EGFR therapy agent approved for the treatment of HNSCC. However, despite the clearly documented clinical benefits of cetuximab, attempts to define a predictive biomarker to stratify patients for treatment with the antibody have been unsuccessful. Remarkably, measuring levels of EGFR protein expression or receptor activation (e.g. the presence of activating gene mutations) have not demonstrated any predictive value benefit to cetuximab treatment in HNSCC. In the context of radical, curative radiotherapy/chemoradiotherapy, dichotomising EGFR expression into low vs high

levels (defined as < or >50% positive cells in the trial with radiotherapy and < or >80% positive cells in the RTOG0522 study with chemoradiotherapy), did not predict benefit from the addition of cetuximab (*2,7,8*). Similarly, in the EXTREME trial of first-line use of platin/5-FU/cetuximab in relapsed/metastatic disease, outcomes were essentially identical for patients with < or >40% EGFR-positive tumor cells (*9*). As a consequence, at present the clinical use of cetuximab is not based on the measurement of intra-tumoral EGFR expression or, indeed, any other biomarker. Against this background, it is important to consider the context in which EGFR has been assessed in previous clinical studies, in order to understand the limitations of the methodologies employed. At this moment, no serum biomarker has been identified that could consistently classify an EGFR+ve subgroup of patients for targeted therapies, so in most clinical trials, EGFR expression has been measured via immunohistochemical staining before the initiation of therapy at a single, static time point, and on a relatively small tissue sample (*10*). For patients with relapsed/metastatic disease, the assessment may have been performed on archival specimens and furthermore, the reported immunohistochemistry data are subject to variability in the sensitivity and specificity of reagents, the use of different staining protocols and concerns relating to the tissue sample that could have provided an unrepresentative view of heterogeneous receptor expression. Therefore, we hypothesized that incorporating imaging with EGFR-specific radioligands into routine clinical practice may not only facilitate a non-invasive, real-time measurement of EGFR expression across the patient's entire tumor burden, but also allow for dynamic monitoring of cetuximab-mediated receptor downregulation providing a marker for adequate treatment dosing.

To date, the use of EGFR-specific molecular imaging for HNSCC patients has been limited to radiolabeled mAbs. And even though, they have demonstrated high uptake in EGFR+ve tumors, their large molecular size (~ 150 kDa) and consequential slow hepatobiliary clearance (e.g. cetuximab half-life in humans is about 95 h) resulted in poor contrast between tumor and normal tissues on images acquired at earlier time points (*11,12*). Accordingly, using smaller molecules, such as mAb fragments (e.g. $F(ab')_2$, Fab'), nanobodies (~15 kDa), or Affibody scaffolds (~7 kDa) that are characterized by rapid tumor penetration and fast blood clearance, could facilitate high-contrast imaging as early as a few hours post-injection (*13*). Indeed, these favourable pharmacokinetics have been demonstrated by PET imaging of EGFR-expressing xenografts using EGFR specific Affibody molecules conjugated to several radioisotopes such as, fluorine-18 (*14,15*), zirconium-89 (*16,17*) and carbon-11 (*18*). Of note, a study by Garousi et al. recently showed greater tumor-to-blood ratios 3 h post-administration of $^{89}$Zr-DFO-$Z_{EGFR:2377}$ in comparison to 48 h post-injection of $^{89}$Zr-DFO-cetuximab, highlighting the advantage of imaging with smaller molecules (*19*).

Herein, we report the use of a radiolabeled Affibody molecule ($Z_{EGFR:03115}$) to non-invasively measures differences in EGFR expression, both *in vitro* and in subcutaneous HNSCC xenograft models. A $^{89}$Zr-labeled conjugate was used to assess tumor-to-organ ratios at different time points and a $^{18}$F-labeled analogue to measure the response to cetuximab treatment *in vivo*. These data support the hypothesis that a targeted-PET agent can quantify EGFR expression level and may represent a powerful missing tool that will facilitate informed image-guided anti-EGFR therapeutic strategies in the clinic.

## MATERIALS AND METHODS

### Cell Lines

Human head and neck cancer cell line HN5 (EGFR++++) was provided by Professor Kevin Harrington (The Institute of Cancer Research, London, UK), CAL27 (EGFR+++), Detroit562 (EGFR++) cell lines and the human breast adenocarcinoma cell line MCF7 (EGFR+) were purchased from the American Type Culture Collection (ATCC, USA). Cells were cultured in DMEM (Gibco, Life Technologies, UK) supplemented with 10% heat-inactivated fetal bovine serum (FBS) (Gibco, Life Technologies, UK) and grown as monolayers at 37°C in a humidified atmosphere containing 5% $CO_2$.

### Preparation of $Z_{EGFR:03115}$-DyLight633, $^{89}$Zr-DFO- and $^{18}$F-AlF-NOTA Affibody Conjugates

The conjugation of DyLight633, DFO-maleimide and maleimidoethylmonoamide NOTA to the Affibody molecules, the consequent $^{89}$Zr and $^{18}$F-AlF radiolabeling procedures are described in the Supplemental Data.

### Flow Cytometry Analysis of EGFR Expression

To assess the EGFR expression in the HN5, CAL27, Detroit562, and MCF7, cell lines, samples were incubated for 1 hour at 4°C with either a fluorescein isothiocyanate (FITC)-conjugated EGFR-specific antibody (20 nM) (Santa Cruz Biotechnology, TX). Afterwards, the cells were washed in PBS and analyzed on the BD™ LSRII flow cytometer (Becton Dickinson, NJ). The results were analyzed using FlowJo v10 (FlowJo, LLC).

## Confocal Microscopy

The binding specificity of the Affibody molecule to EGFR was assessed by incubating HN5 cells with $Z_{EGFR:03115}$-Dylight633 (1 μM) for 1 h at 37°C with and without pre-incubation with 100-fold excess of the $Z_{EGFR:03115}$. To study the internalization of the conjugate HN5 cells were incubated with $Z_{EGFR:03115}$-Dylight633 (1 μM) for 1 h at 37°C, washed with PBS, and confocal images were acquired at 3, 8 and 24 h post-incubation. All cells were counterstained with Hoechst®33342 (nuclear stain; Thermo Fisher Scientific, UK) and Lysotracker™ Green DND-26 (lysosome stain; Thermo Fisher Scientific, UK) 1 h before capturing the images using the Zeiss LSM700 confocal microscope (Carl Zeiss Inc, Germany). Images (8 bit, 1024 x 1024) were analyzed using the Zen2009 software (Zeiss, Germany).

## Immunoblotting

Western blotting was carried out as previously described in the literature (*20*). Briefly, the proteins were immunoblotted with primary antibodies against EGFR, p-EGFR (Tyr1068), AKT (Protein kinase B), p-AKT (S473), β-Actin or GAPDH (all from Cell Signaling Technology, UK,) overnight at 4°C. On the following day, membranes were rinsed and incubated with horseradish peroxidase-conjugated secondary antibodies (Cell Signaling Technology, UK) for 1 h at RT. The immunoblots were visualized following the addition of SuperSignal™ West Pico PLUS Chemiluminescent Substrate (Thermo Fisher Scientific, UK) and imaged with a ChemiDoc™ XRS+ System (Bio-Rad, UK). The densitometry was performed using ImageJ (NIH, WA).

## *In vitro* Binding Affinity and Specificity

The disassociation constants ($K_d$) of $^{89}$Zr- and $^{18}$F-AlF-based $Z_{EGFR:03115}$ conjugates were assessed by a saturation binding assay. The CAL27 cells were incubated with increasing concentrations of radiolabeled $Z_{EGFR:03115}$ (0.1 – 50 nM) for 2 h at 4°C. Non-specific binding was determined by adding 100-fold excess of unlabeled $Z_{EGFR:03115}$. Cell-bound radioactivity was determined using the 2480WIZARD$^2$ Automatic Gamma Counter (PerkinElmer, UK). To estimate the $K_d$, the data were plotted as the amount of bound (nM) *vs.* ligand (nM). The specific binding was measured by subtracting the fraction of the non-specific from the total binding, and fitted using a nonlinear regression curve, one-site specific receptor-binding model using GraphPad Prism v7.0 Software (San Diego, CA).

To evaluate the binding specificity of $Z_{EGFR:03115}$, HN5, CAL27, Detroit562 and MCF7 cells were incubated with either $^{89}$Zr-DFO-$Z_{EGFR:03115}$ or $^{18}$F-AlF-NOTA-$Z_{EGFR:03115}$ (20 nM) for 1 h at 4°C. To some of the cells, a 100-fold excess of either cetuximab (Merck, Global, Germany), natural EGF ligand (Thermo Fisher Scientific, UK) or unlabeled $Z_{EGFR:03115}$ were added. Afterwards, cells were rinsed, trypsinized and the radioactivity was measured using a γ-counter. Each experiment was normalized to the maximum cell-associated radioactivity and presented as the mean of n = 3 independent experiments (performed in triplicate) ± SEM.

**Biodistribution**

All experiments were performed in compliance with licenses issued under the UK Animals (Scientific Procedures) Act 1986. Studies were compliant with the United Kingdom National Cancer Research Institute Guidelines for Animal Welfare in Cancer Research (*21*). Female NU(NCr)-Foxn1$^{nu}$ mice were purchased from Charles River

Laboratories, UK. To generate tumor xenografts, CAL27 ($4x10^6$), Detroit562 ($6x10^6$) or MCF7 ($6.5x10^6$) cells were inoculated in BD Matrigel™ Matrix subcutaneously into the shoulder of the mouse. For the MCF7 xenograft model, a 17β-estradiol pellet/mouse (0.72 mg, 90-day release) was implanted 48 h before cell inoculation. The tumors were allowed to grow until reaching an approximate volume of 100 $mm^3$.

Dose-dependent $^{89}$Zr-DFO-$Z_{EGFR:03115}$ uptake was assessed by injecting the $^{89}$Zr-DFO- $Z_{EGFR:03115}$ into the tail vein (2 μg) either together or 30 mins after increasing amounts of unlabeled Affibody molecule (1, 5, 10, 15 and 20 μg). $^{89}$Zr-$Z_{Taq}$ (3-3.1 MBq, 2μg) was used as a negative control. Animals were sacrificed at 3, 24 and 48 h post-injection. Blood was collected and the major organs were excised, weighed and their associated radioactivity was measured, using a γ-counter. Unless otherwise stated, the results for each tissue sample were calculated as percentage of the injected dose per gram of tissue (%ID/g) (n ≥ 3 mice ± SD).

**Autoradiography**

Dissected tumors were embedded in an optimal-cutting-temperature compound (Tissue-Tek, USA) and immediately snap frozen on dry ice. The specimens were sectioned to a thickness of 6 μm using a cytomicrotome (Thermo Fisher Scientific, UK) and mounted on slides. The slides were exposed to a photostimulable phosphor plate for 24 h and read using a Typhoon7000 phosphorimager (GE Healthcare Life Sciences, UK). The recorded images were analyzed using ImageQuant TL Version 8.1 (GE Healthcare Life Sciences, UK).

## Immunohistochemistry

Tumors were fixed in formalin and paraffin-embedded to be sectioned and further processed (Breast Cancer Now Histopathology Core Facility, London). Multiple sections were taken at regular intervals across each tumor, stained with H&E (Leica, Germany) and an anti-EGFR mAb (Dako pharmDx$^{TM}$, UK) according to the manufacturer's protocol and imaged with the NanoZoomer-XR (Hamamatsu Photonics, Japan).

## PET Imaging

Mice were anaesthetized using isoflurane (1.5%–2% v/v in $O_2$) before imaging. Using an Albira PET/SPECT/CT preclinical imaging system (Bruker, UK), whole body 15 min ($^{89}$Zr) or 10 min ($^{18}$F) static images were acquired with an energy window of 358 to 664 keV, followed by CT acquisition. PET data were reconstructed using an MLEM algorithm (12 iterations), scatter and attenuation corrections were applied using their respective CTs. High resolution CT scans were performed with the X-ray tube set-up at a voltage of 45 kV, current of 400 μA, 250 projections (1 sec per projection) and a voxel size of 0.5×0.5×0.5 mm$^3$. The CT images were reconstructed using a filtered back projection algorithm. The PMOD software package (PMOD Technologies Ltd, CH) was used to analyze the images. The tumor volume was selected by first drawing volumes of interest around the tumor and selecting a 50% maximum pixel isocontour. The mean counts were extracted and converted into %ID/g using a calibration factor (MBq/g/counts) calculated by scanning a source ($^{89}$Zr or $^{18}$F) of known activity and volume.

## Cetuximab Treatment

Cetuximab treatment studies were conducted using HN5 xenografts, as this model is particularly sensitive to cetuximab treatment (*22*). Mice were randomized into either control ($n$ = 6) or treatment ($n$ = 7) groups and treated with a vehicle or cetuximab, respectively. The control mice were injected with $^{18}$F-AlF-NOTA-Z$_{EGFR:03115}$ (12 μg, 1.5-2 MBq/mouse), imaged 1 h post-conjugate administration, and sacrificed for biodistribution study. Mice from the treatment group underwent cetuximab treatment (600 μg bolus injection every 3 days for a total of 4 doses delivered via intraperitoneal injection). Allowing 13 days for post-treatment clearance of the mAb, subsequent PET images were acquired with $^{18}$F-AlF-NOTA-Z$_{EGFR:03115}$ (12 μg, 1.5-2 MBq/mouse). In addition, to demonstrate a lack of competition between the Affibody and remaining cetuximab in the blood circulation, an extra group of mice (n = 3) was co-injected with cetuximab (3.75 μg, 26 pmol) an amount which was estimated to still be present in the blood 13 days after completion of treatment, considering a mAb biological half-life of 40 h. Densitometric analysis of the tumor tissue lysates was performed using ImageJ (NIH, USA). Data are presented as means ± SEM (blots n = 2).

## Statistical Analysis

Statistical analyses were performed using Prism software (GraphPad Software v7.0).

Significance was determined using unpaired two-tailed Student's t test with Welch's correction. In order to determine statistical significance between uptakes in the different xenograft models, a two-way ANOVA with Tukey correction was used. Correlation analysis was performed using Spearman's rank correlation, with linear regression, 95%

confidence intervals. Statistically significant differences between groups were assumed if $P \leq 0.05$. No data were excluded from the analysis.

## RESULTS

### $Z_{EGFR:03115}$ Targeting Properties

Initially, EGFR expression was determined in the selected cancer cell lines by Western blot and flow cytometry. The Western blotting results revealed varying levels of EGFR expression, from high, HN5 (EGFR++++); through medium, CAL27 (EGFR+++); to low, Detroit562 (EGFR++) and negligible in MCF7 (EGFR+) (Supplementary Fig. 1), which was concordant with the flow cytometry data using $Z_{EGFR:03115}$-Dylight633 (Fig. 1A).

To demonstrate that $Z_{EGFR:03115}$ specifically targets EGFR, HN5 cells were incubated with $Z_{EGFR:03115}$-Dylight633 and the cell-associated fluorescence was visualized by confocal microscopy. After a 1 h incubation at 37°C, intense fluorescent signal was found on the cell membrane (Fig. 1B). Images acquired 3, 8 and 24 h later showed an intracellular accumulation of the conjugate, although the vast majority still remained bound to the membrane, even 24 h post-incubation (Fig. 1C). Additionally, incubating the cells with 100-fold excess of unlabeled $Z_{EGFR:03115}$ markedly decreased the fluorescence signal (Fig. 1B bottom panel) demonstrating that binding is EGFR specific and receptor-mediated.

### *In vitro* Binding of $^{89}$Zr-DFO-$Z_{EGFR:03115}$

The disassociation constant ($K_d$) and maximum number of binding sites ($B_{max}$) of $^{89}$Zr-DFO-$Z_{EGFR:03115}$ were determined by a cell-based saturation assay using CAL27

cells. The calculated $K_d$ and $B_{max}$ values were found to be 5.00 ± 0.3 nM and (3.71 ± 0.05)×$10^6$ sites/cell, respectively (Fig. 2A). The target-binding specificity of $^{89}$Zr-DFO-$Z_{EGFR:03115}$ was evaluated in a panel of cancer cell lines with different EGFR expression, demonstrating the cell-associated radioactivity was consistent with the measured total EGFR protein expression level in each cell line (Fig. 2B and Fig. 1A). Importantly, blocking the receptor with 100-fold excess of non-labeled $Z_{EGFR:03115,}$ cetuximab or the natural ligand EGF, which were demonstrated to compete with the Affibody molecule for the same binding site, significantly reduced radioactivity signal, further confirming the specificity of $^{89}$Zr-DFO-$Z_{EGFR:03115}$ for the target (Fig. 2B).

**Protein Dose-Escalation Studies**

Protein dose-escalation studies were initially performed to test the bioavailability of the radioconjugate for tumor targeting. By adding increasing amounts of non-labeled Affibody molecule (1, 5, 10, 15, 20 μg) to the $^{89}$Zr-DFO-$Z_{EGFR:03115}$ (2 μg, 2.5-3.4 MBq/mouse), the radioactivity signal in the liver significantly decreased from 20.74 ± 8.31 to 3.19 ± 0.14 %ID/g (Table 1). Concurrently, tumor uptake increased from 1.75 ± 0.21 to 3.69 ± 1.19 %ID/g (Table 1, Fig. 3). Importantly, an insignificant uptake was achieved when the non-specific Affibody-based radioconjugate ($^{89}$Zr-DFO-$Z_{Taq}$) was injected in CAL27 tumors (0.26 ±0.05 %ID/g) (Table 1, Supplementary Fig. B2). Also, no significant differences in tumor uptake (3.69 ± 1.19 %ID/g vs 3.88 ± 0.46 %ID/g) were found when non-labeled $Z_{EGFR:03115}$ was either injected 30 min before the radioconjugate or co-injected with the $^{89}$Zr-DFO-$Z_{EGFR:03115}$ (Supplementary Fig. 2). Therefore, the protein dose of 10 μg was administered alongside the radioconjugate for

further studies, as it provided the best contrast between targeted and non-targeted tissues (tumor-to-background ratio of 10.25 at 3 h post-injection).

### $^{89}$Zr-DFO-Z$_{EGFR:03115}$ Pharmacokinetics

The pharmacokinetics of the $^{89}$Zr-DFO-Z$_{EGFR:03115}$ were evaluated by performing biodistribution studies at 3, 24 and 48 h post-injection of 2 μg (2.5-3.4 MBq) of radioconjugate with 10 μg of Z$_{EGFR:03115}$. The tumor/muscle (T/M) and tumor/blood (T/B) ratios at 3 h were 10.31 and 1.04, respectively. Due to clearance from non-specific organs, both values increased at 24 h and 48 h post-injection with T/M of 17.35 and 13.56 and T/B of 2.79 and 9.34, respectively (Table 2). At the same time, tumor uptake decreased from 3.88 ± 0.46 %ID/g at 3 h to 2.43 ± 0.27 %ID/g and 2.13 ± 0.12 %ID/g at 24 and 48 h, respectively. As the higher tumor uptake would allow for better differentiation between the xenograft tumor types we therefore decided to perform the proceeding studies at 3 h post-injection. As expected, the kidney uptake remained relatively high over time (104.85 ± 11.10 %ID/g even after 48 h) as a result of glomerular filtration of the Affibody molecule followed by reabsorption, degradation and retention in proximal tubular cells. Additionally, as expected when using $^{89}$Zr-labeled agents radioactivity accumulation in the bone at 24 h (2.28 ± 0.27 %ID/g) and 48 h (3.44 ± 0.59 %ID/g), was detected.

### Correlation of $^{89}$Zr-DFO-Z$_{EGFR:03115}$ Tumor Uptake and EGFR Expression

To evaluate whether $^{89}$Zr-DFO-Z$_{EGFR:03115}$ could distinguish between tumors with varying EGFR expression levels, mice bearing CAL27, Detroit562 and MCF7 xenografts received the radiotracer (2 μg co-injected with 10 μg of Z$_{EGFR:03115}$; 2.4-3.4 MBq/mouse)

and were imaged 3 h post-injection using PET/CT. The quantified PET imaging data indicated that the highest levels of radioconjugate accumulation were in CAL27 tumors (4.73 ± 0.90 %ID/g), (Fig. 4A and Fig. 4B). Importantly, *in vivo* specificity of $Z_{EGFR:03115}$ was confirmed by the lower $^{89}$Zr-DFO-$Z_{EGFR:03115}$ uptake in low EGFR expressing MCF7 xenografts (1.41 ± 0.20 %ID/g). These data were then corroborated by the corresponding biodistribution results (Fig. 4B). Furthermore, tumor targeting by the radioconjugate correlated with EGFR expression measured *ex vivo* by Western blot analysis and immunohistochemical staining (Fig. 4C Top, Supplementary Fig. 3). In addition, the autoradiography of tissue slices from CAL27 and Detroit562 tumors confirmed marked differences in $^{89}$Zr-DFO-$Z_{EGFR:03115}$ uptake as compared to MCF7 tumors (Fig. 4C Bottom).

**Monitoring Cetuximab-Induced *in vivo* EGFR Downregulation**

To monitor the response to cetuximab treatment, the long-lived isotope, zirconium-89 ($T_{1/2}$ = 78.4 h), was replaced with fluorine-18 ($T_{1/2}$ = 108 min). *In vitro* characterization of $^{18}$F-AlF-NOTA-$Z_{EGFR:03115}$ confirmed the high affinity ($K_d$ = 5.4 ± 1.1 nM) and specificity of the radioconjugate for EGFR (Supplementary Fig. 4). Following $^{18}$F-AlF-NOTA-$Z_{EGFR:03115}$ intravenous administration into mice bearing HN5 tumors, a significantly lower tumor uptake was observed in cetuximab-treated mice in comparison to control HN5 tumors, as shown both by the PET image quantification (6.29 ± 0.89 %ID/g vs 2.37 ± 0.31 %ID/g) and the biodistribution data (6.18 ± 0.38 %ID/g vs 0.80 ± 0.17 %ID/g) (Fig. 5; Supplementary Fig. 5A). PET quantification of the cetuximab-treated mice yielded a slightly higher %ID/g than the biodistribution studies, which is likely due to the relatively high radioactivity in the blood at 1 h post-injection

(Supplementary Fig. 5B and 5C). However, when background subtraction was applied, only a small amount of the activity was present in the treated tumors (0.28 ± 0.26% ID/g) (Supplementary Fig. 5D). This significant decrease in the radioconjugate accumulation correlated with a downregulation of EGFR expression following cetuximab treatment as assessed by Western blot ($r = 0.961$, $P < 0.0001$) (Fig. 6A and B, Supplementary Fig. 5E and 5F). Furthermore, discernible differences in phosphorylated EGFR and AKT were observed between control and treated mice (Fig. 6A). Additionally, a cetuximab-induced decrease in EGFR expression was confirmed by the immunohistochemistry (Fig. 6C). No significant change in tumor uptake was measured when a group of mice were injected with $^{18}$F-AlF-NOTA-$Z_{EGFR:03115}$ and a quantity of cetuximab which was estimated to be still circulating in the blood 13 days post-treatment (Supplementary Fig. B5F). This confirmed that the decrease in tumor uptake was not due to the mAb competing for the same epitope on the receptor. Additionally, no significant decrease in tumor uptake was measured (Supplementary Fig. 5G).

## DISCUSSION

Despite evidence demonstrating an important prognostic role for EGFR in HNSCC, receptor expression is not predictive of response to EGFR-targeted therapy. This is potentially due to EGFR expression being evaluated in the major clinical trials by an immunohistochemistry-based scoring system, which may not reflect the heterogeneous receptor expression of the whole tumor mass and associated regional lymph node metastases. The integration of molecular imaging biomarkers into standard clinical protocols could address these limitations, providing a global representation of

tumor target expression and accessibility, enabling for image-guided selection of patients for EGFR-targeted therapies.

Recently, therapeutic mAbs targeting EGFR have been radiolabeled with multiple radioisotopes to provide information about tumor targeting, pharmacokinetics and accumulation in critical normal organs (*23-25*). Even et al. reported that $^{89}$Zr-cetuximab-PET shows large inter-patient variability in locally advanced head and neck squamous cell carcinomas and provides additional information about the accessibility of the drug into the tumor when compared with $^{18}$F-FDG-PET and EGFR expression evaluated by *ex vivo* methods (*26*). However, Niu et al. have demonstrated in different HNSCC xenografts that poor $^{64}$Cu-DOTA-panitumumab delivery may result in the lack of correlation between PET quantification and the EGFR protein expression (*27*).

We, therefore, utilized a low molecular weight targeting vector (i.e. Affibody molecule), as the rapid extravasation from the blood vessels and enhanced tumor mass penetration, would provide favorable pharmacokinetics for imaging applications and facilitate the visualization of tumor regions inaccessible for mAb, particularly at early time points. In fact, van Dijk et al. have recently shown high and specific uptake of $^{111}$In-cetuximab-F(ab')$_2$ as early as 4 h post-injection, with high imaging contrast at 24 h in FaDu xenografts. The authors additionally reported that the radioconjugate can monitor the effects of EGFR inhibition combined with irradiation in head and neck carcinoma models (*23,28*). However, EGFR targeting mAb fragments do not bind to murine EGFR, which limits the proper evaluation of the real tumor-to-background signal of these agents in preclinical models. To address this limitation, several recent studies, have investigated whether EGFR-specific Affibody molecules, which cross-react with EGFR of mouse origin, can delineate EGFR+ve tumors and provide high-contrast tumor

imaging in the presence of endogenous background levels of EGFR (*15-17*). In our study, we investigated the binding of $Z_{EGFR:03115}$ in a panel of HNSCC models. The *in vitro* data clearly demonstrated that the fluorescent ($Z_{EGFR:03115}$-Dylight633) and radio-labeled ($^{89}$Zr-DFO-$Z_{EGFR:03115}$, $^{18}$F-AlF-NOTA-$Z_{EGFR:03115}$) Affibody-based conjugates maintained a high binding affinity for EGFR and enabled the detection of differences in EGFR expression. The specificity for EGFR binding was confirmed by blocking assays with cetuximab and the natural ligand, EGF. To study the pharmacokinetics of $Z_{EGFR:03115}$ at later time points we radiolabeled the Affibody molecule with a long lived PET radioisotope (*17*). A $^{89}$Zr was seen as a better-suited radionuclide than $^{124}$I for such studies since radiometals are retained more readily in cells than radiohalogens.

Numerous studies have highlighted the importance of optimizing the protein dose when targeting EGFR in order to partially saturate endogenous EGFR expression in the liver and, subsequently, increase the tumor uptake (*29,30*). Therefore, we performed a protein dose-escalation study and found we can clearly visualize the tumor 3 h post co-injecting 10 μg of $Z_{EGFR:03115}$ alongside $^{89}$Zr-DFO-$Z_{EGFR:03115}$ (T/M ratio of 10.31). Furthermore, radioconjugate tumor accumulation was confirmed to be EGFR specific, as PET imaging of MCF-7 (EGFR+) showed much lower accumulation of the radioconjugate than tumors with higher receptor expression. Moreover, the $^{89}$Zr-DFO-$Z_{Taq}$-related radioactivity in the CAL27 tumor (EGFR++++) was negligible. Importantly, the accumulation of $^{89}$Zr-DFO-$Z_{EGFR:03115}$ in the tumor correlated with EGFR protein expression level, assessed *ex vivo* by tumor tissue lysates and EGFR staining of tumor sections derived from xenograft models with various levels of receptor expression. Our results successfully demonstrated the advantage of performing imaging at later time points with the Affibody molecule, as exemplified by the increase in tumor-to-

background ratios. However, the decrease in tumor accumulation following the 3 h post-injection would limit the sensitivity for discerning subtle changes in EGFR expression. Therefore, the 3 h time point was selected to compare the receptor levels between the xenograft models. Furthermore, the clinical use of an Affibody conjugate radiolabeled with $^{18}$F would be more suitable than $^{89}$Zr, due to a lower radiation exposure burden to the patient, a more desirable positron branching ratio and a shorter radioactive half-life ($T_{1/2}$ = 108 min vs 78.4 h). We postulated that $^{18}$F-AlF-NOTA-$Z_{EGFR:03115}$ could measure dynamic changes in receptor expression in response to EGFR inhibition.

This may provide useful information for adaptive treatment schedules with anti-EGFR mAbs, since current dosing of cetuximab is based on the patient's weight and the only confirmed clinical variable that predicts response to this agent is the grade of skin toxicity that occurs after treatment initiation (*31,32*). Notably, following cetuximab treatment, we observed a significantly lower radioconjugate uptake in the group of mice treated with this mAb. Moreover, this change was in line with decreased EGFR protein levels evaluated by Western blot and immunohistochemistry. These results, together with the fact that no significant change in tumor volume was observed during the treatment, highlight the potential for utilizing EGFR imaging as a tool for assessing cetuximab efficacy based on the receptor level rather than purely relying on anatomical imaging. Of note, EGFR downregulation, due to the internalization and subsequent degradation of EGFR in lysosomes, has recently been reported to be an important determinant of the efficacy of cetuximab treatment for colorectal cancer (*33*). Our data suggest that it may be possible to evaluate this effect non-invasively using PET-based imaging with radiolabeled Affibody molecule.

Furthermore, immunostaining of tumor sections revealed the presence of residual EGFR positive cells that directly reflected their viability following cetuximab treatment. These results were corroborated by incomplete inhibition of pAKT signaling. The surviving cell populations were likely inaccessible for the bulky antibody, but potentially may have evaded cetuximab treatment by activating compensatory signaling pathways. However, we recognize that further investigations are needed to verify these findings, which may point the way to further treatment options for such tumors. In the future $^{18}$F-AIF-NOTA-$Z_{EGFR:03115}$ could also be utilized for the identification of residual EGFR-positive cells that may be responsible for subsequent cancer relapse.

In summary, our results demonstrate that non-invasive molecular imaging of EGFR may open the door for guiding selection and monitoring of anti-EGFR targeted therapy dosing plans before tumor response, as measured by changes in tumor volumes on conventional cross-sectional imaging modalities, is detected. Such an approach may spare patients unnecessary toxicities and improve EGFR-targeted therapy by tailoring a more personalized treatment.

**Acknowledgments**

The authors gratefully thank AffibodyAB for supplying the Affibody molecules. We thank the Pathology Core Facility for immunohistochemistry assistance.

## REFERENCES

1. Vigneswaran N, Williams MD. Epidemiologic trends in head and neck cancer and aids in diagnosis. *Oral Maxillofac Surg Clin North Am.* 2014;26:123-141.

2. van Dijk LK, Boerman OC, Kaanders JH, Bussink J. PET Imaging in Head and Neck Cancer Patients to Monitor Treatment Response: A Future Role for EGFR-Targeted Imaging. *Clin Cancer Res.* 2015;21:3602-3609.

3. Leemans CR, Braakhuis BJ, Brakenhoff RH. The molecular biology of head and neck cancer. *Nat Rev Cancer.* 2011;11:9-22.

4. Kalyankrishna S, Grandis JR. Epidermal growth factor receptor biology in head and neck cancer. *Journal of Clinical Oncology.* 2006;24:2666-2672.

5. Kang H, Kiess A, Chung CH. Emerging biomarkers in head and neck cancer in the era of genomics. *Nat Rev Clin Oncol.* 2015;12:11-26.

6. Rao SD, Fury MG, Pfister DG. Molecular-targeted therapies in head and neck cancer. *Semin Radiat Oncol.* 2012;22:207-213.

7. Bonner JA, Harari PM, Giralt J, et al. Radiotherapy plus cetuximab for locoregionally advanced head and neck cancer: 5-year survival data from a phase 3 randomised trial, and relation between cetuximab-induced rash and survival. *Lancet Oncol.* 2010;11:21-28.

8. Ang KK, Zhang Q, Rosenthal DI, et al. Randomized Phase III Trial of Concurrent Accelerated Radiation Plus Cisplatin With or Without Cetuximab for Stage III to IV Head and Neck Carcinoma: RTOG 0522. *Journal of Clinical Oncology.* 2014;32:2940-2950.

9. Cohen MH, Chen H, Shord S, et al. Approval summary: Cetuximab in combination with cisplatin or carboplatin and 5-fluorouracil for the first-line treatment of

patients with recurrent locoregional or metastatic squamous cell head and neck cancer. *Oncologist.* 2013;18:460-466.

10. Asgeirsson KS, Agrawal A, Allen C, et al. Serum epidermal growth factor receptor and HER2 expression in primary and metastatic breast cancer patients. *Breast Cancer Res.* 2007;9:R75.

11. Fracasso PM, Burris H, Arquette MA, et al. A phase 1 escalating single-dose and weekly fixed-dose study of cetuximab: Pharmacokinetic and pharmacodynamic rationale for dosing. *Clinical Cancer Research.* 2007;13:986-993.

12. van Dongen GAMS, Visser GWM, Hooge MNLD, De Vries EG, Perk LR. Immuno-PET: A navigator in monoclonal antibody development and applications. *Oncologist.* 2007;12:1379-1389.

13. Lofblom J, Feldwisch J, Tolmachev V, Carlsson J, Stahl S, Frejd FY. Affibody molecules: engineered proteins for therapeutic, diagnostic and biotechnological applications. *FEBS Lett.* 2010;584:2670-2680.

14. Miao Z, Ren G, Liu H, Qi S, Wu S, Cheng Z. PET of EGFR expression with an 18F-labeled affibody molecule. *J Nucl Med.* 2012;53:1110-1118.

15. Su X, Cheng K, Jeon J, et al. Comparison of two site-specifically (18)F-labeled affibodies for PET imaging of EGFR positive tumors. *Mol Pharm.* 2014;11:3947-3956.

16. Summer D, Garousi J, Oroujeni M, et al. Cyclic versus Noncyclic Chelating Scaffold for (89)Zr-Labeled ZEGFR:2377 Affibody Bioconjugates Targeting Epidermal Growth Factor Receptor Overexpression. *Mol Pharm.* 2018;15:175-185.

17. Burley T, Martins CD, Da Pieve C, et al. 89Zr-Affibody for specific detection of EGFR expression in HNSCC. *Eur J Nucl Med Mol Imaging.* 2015;42:S247-S247.

18. Cheng Q, Wallberg H, Grafstrom J, et al. Preclinical PET imaging of EGFR levels: pairing a targeting with a non-targeting Sel-tagged Affibody-based tracer to estimate the specific uptake. *EJNMMI Res.* 2016;6:58.

19. Garousi J, Andersson KG, Mitran B, et al. PET imaging of epidermal growth factor receptor expression in tumours using 89Zr-labelled ZEGFR:2377 affibody molecules. *Int J Oncol.* 2016;48:1325-1332.

20. Kramer-Marek G, Kiesewetter DO, Capala J. Changes in HER2 expression in breast cancer xenografts after therapy can be quantified using PET and (18)F-labeled affibody molecules. *J Nucl Med.* 2009;50:1131-1139.

21. Workman P, Aboagye EO, Balkwill F, et al. Guidelines for the welfare and use of animals in cancer research. *Br J Cancer.* 2010;102:1555-1577.

22. Boeckx C, Op de Beeck K, Wouters A, et al. Overcoming cetuximab resistance in HNSCC: the role of AURKB and DUSP proteins. *Cancer Lett.* 2014;354:365-377.

23. van Dijk LK, Hoeben BA, Kaanders JH, Franssen GM, Boerman OC, Bussink J. Imaging of epidermal growth factor receptor expression in head and neck cancer with SPECT/CT and 111In-labeled cetuximab-F(ab')2. *J Nucl Med.* 2013;54:2118-2124.

24. Aerts HJWL, Dubois L, Perk L, et al. Disparity Between In Vivo EGFR Expression and (89)Zr-Labeled Cetuximab Uptake Assessed with PET. *Journal of Nuclear Medicine.* 2009;50:123-131.

25. Song IH, Noh Y, Kwon J, et al. Immuno-PET imaging based radioimmunotherapy in head and neck squamous cell carcinoma model. *Oncotarget.* 2017;8:92090-92105.

26. Even AJ, Hamming-Vrieze O, van Elmpt W, et al. Quantitative assessment of Zirconium-89 labeled cetuximab using PET/CT imaging in patients with advanced head and neck cancer: a theragnostic approach. *Oncotarget.* 2017;8:3870-3880.

27. Niu G, Li Z, Xie J, Le QT, Chen X. PET of EGFR antibody distribution in head and neck squamous cell carcinoma models. *J Nucl Med.* 2009;50:1116-1123.

28. van Dijk LK, Boerman OC, Franssen GM, Kaanders JH, Bussink J. 111In-cetuximab-F(ab')2 SPECT and 18F-FDG PET for prediction and response monitoring of combined-modality treatment of human head and neck carcinomas in a mouse model. *J Nucl Med.* 2015;56:287-292.

29. Tolmachev V, Rosik D, Wallberg H, et al. Imaging of EGFR expression in murine xenografts using site-specifically labelled anti-EGFR 111In-DOTA-Z EGFR:2377 Affibody molecule: aspect of the injected tracer amount. *Eur J Nucl Med Mol Imaging.* 2010;37:613-622.

30. de Souza ALR, Marra K, Gunn J, et al. Fluorescent Affibody Molecule Administered In Vivo at a Microdose Level Labels EGFR Expressing Glioma Tumor Regions. *Molecular Imaging and Biology.* 2017;19:41-48.

31. Orditura M, De Vita F, Galizia G, et al. Correlation between efficacy and skin rash occurrence following treatment with the epidermal growth factor receptor inhibitor cetuximab: A single institution retrospective analysis. *Oncology Reports.* 2009;21:1023-1028.

32. Bar-Ad V, Zhang Q, Harari PM, et al. Correlation Between the Severity of Cetuximab-Induced Skin Rash and Clinical Outcome for Head and Neck Cancer Patients: The RTOG Experience. *International Journal of Radiation Oncology Biology Physics.* 2016;95:1346-1354.

33. Okada Y, Kimura T, Nakagawa T, et al. EGFR Downregulation after Anti-EGFR Therapy Predicts the Antitumor Effect in Colorectal Cancer. *Molecular Cancer Research.* 2017;15:1445-1454.

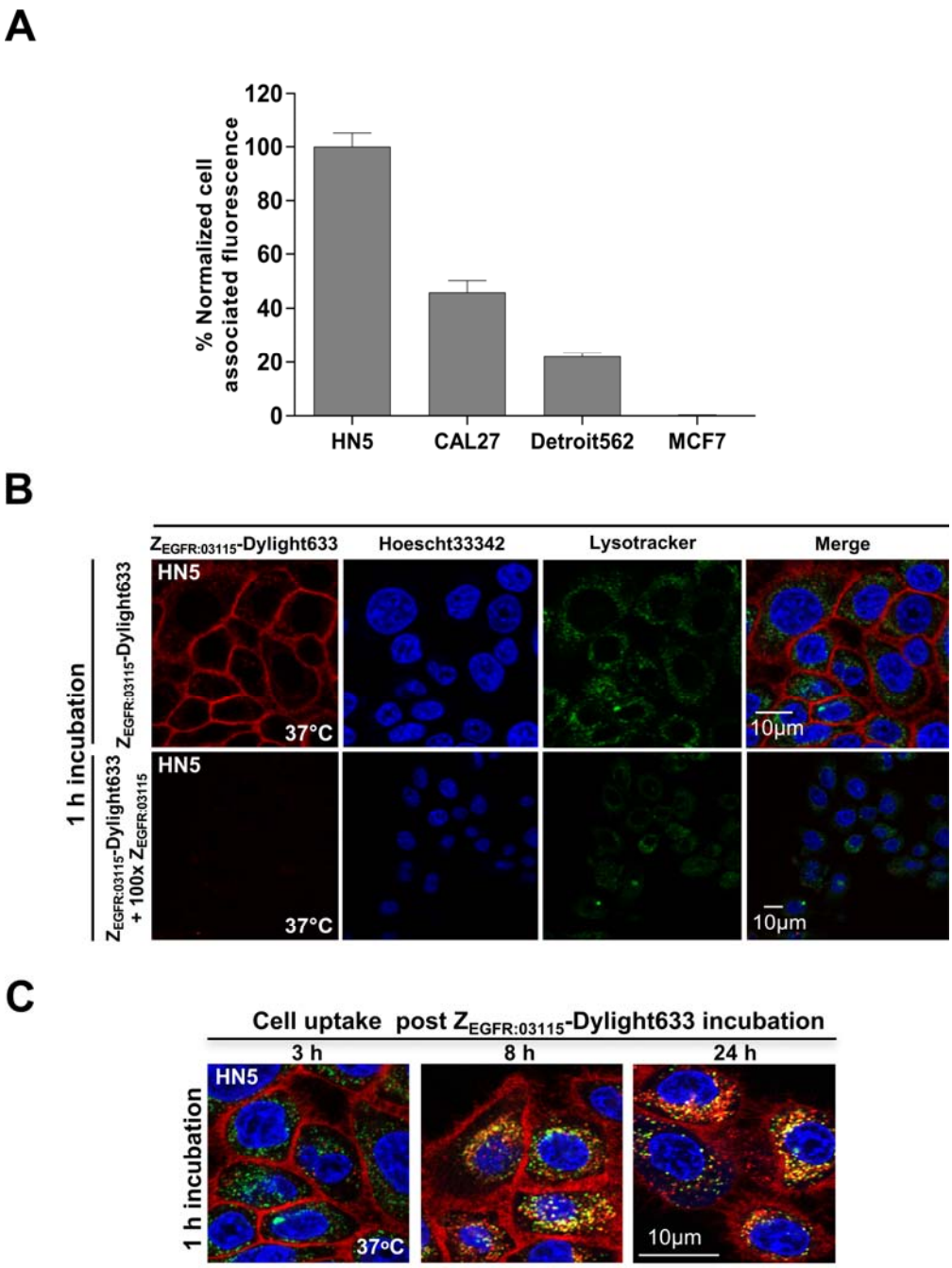


**Figure 1:** EGFR expression as determined by flow cytometry in the selected cancer cell lines (A). *In vitro* binding specificity of $Z_{EGFR:03115}$-Dylight633 in HN5 cells as shown by confocal microscopy (B). Internalization studies of $Z_{EGFR:03115}$-Dylight633 3 h, 8 h and 24 h post 1 h incubation in HN5 cells (C).

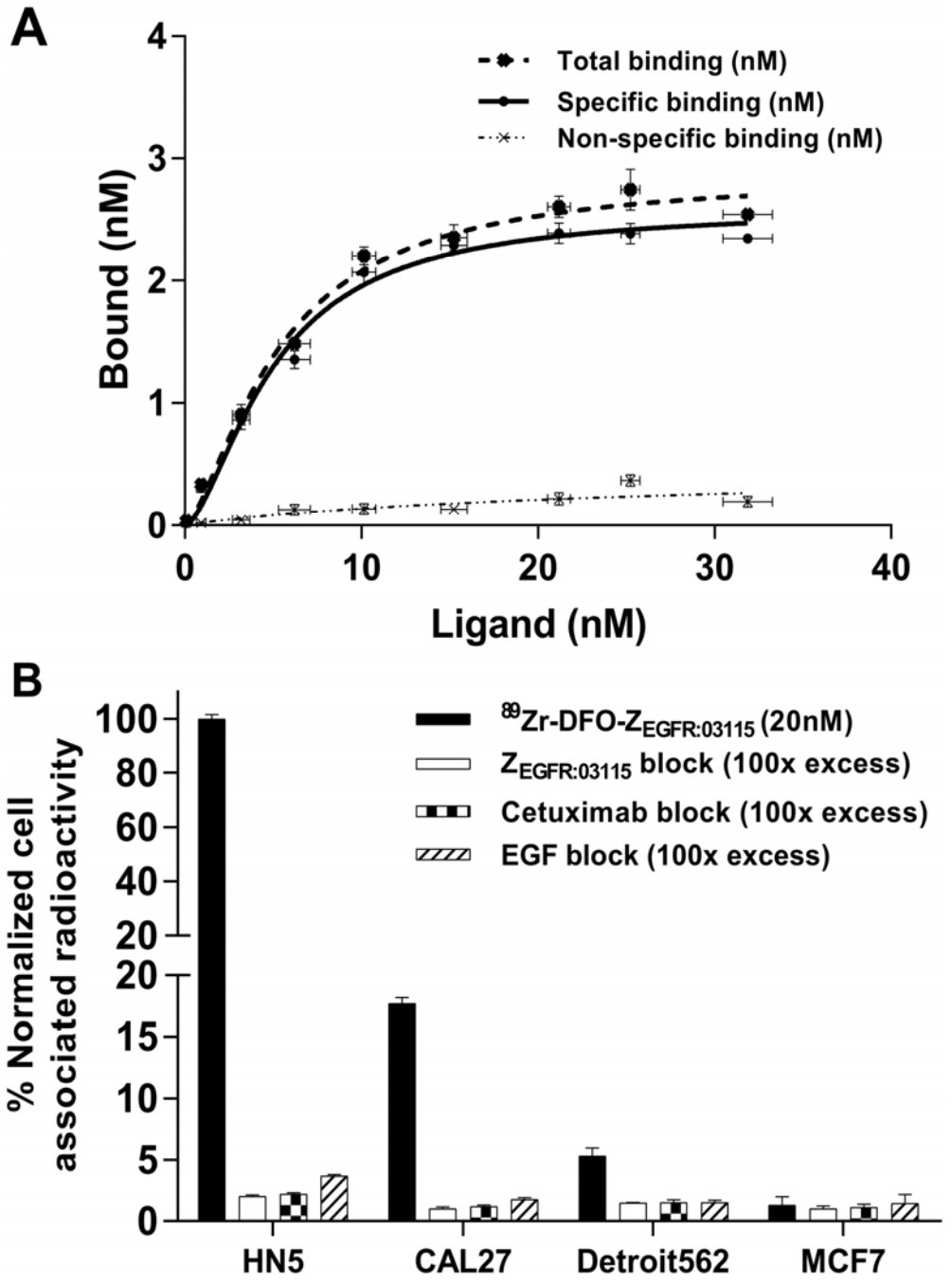


**Figure 2:** Saturation curve obtained for CAL27 cells incubated with increasing concentrations of $^{89}$Zr-DFO-$Z_{EGFR:03115}$ (A). *In vitro* binding specificity of $^{89}$Zr-DFO-$Z_{EGFR:03115}$ in the selected cell lines with and without blocking using unlabeled Affibody, cetuximab or EGF. Data are normalized to the maximum cell-associated radioactivity per experiment (B).

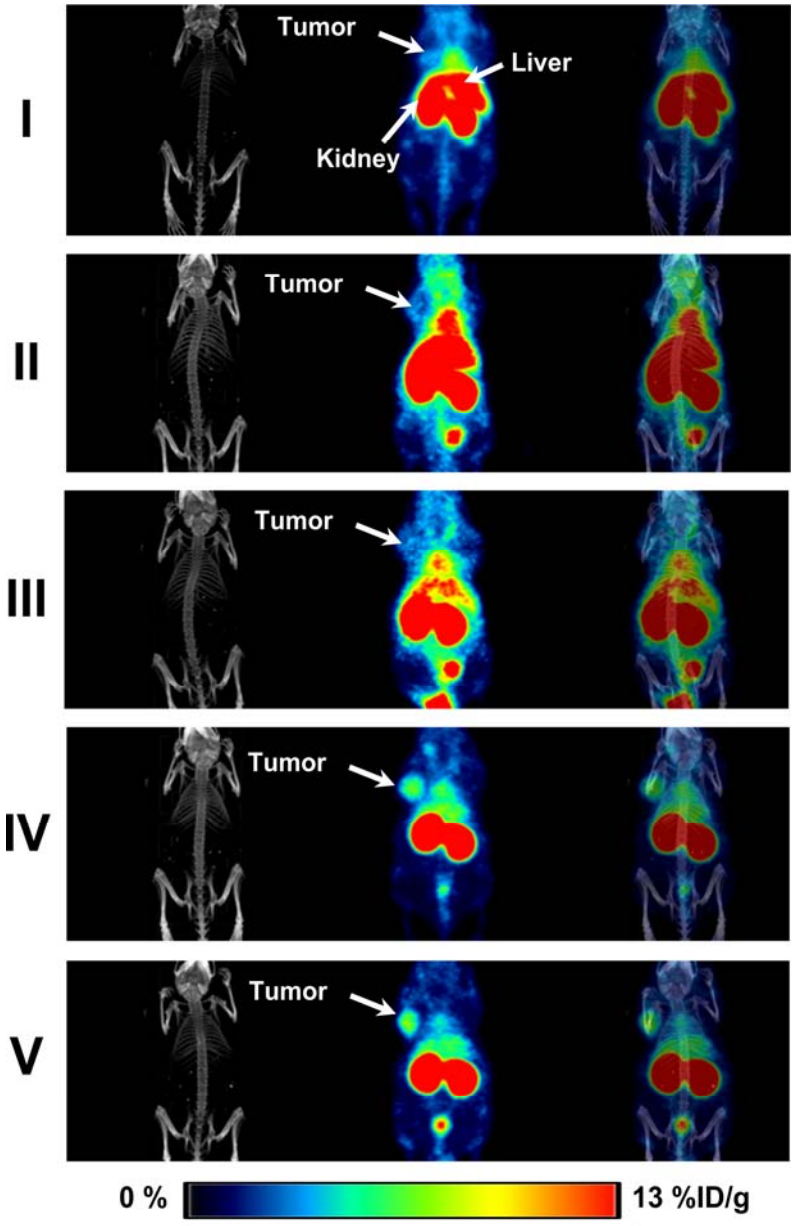


**Figure 3:** Whole-body coronal PET/CT images acquired 3 h after $^{89}$Zr-DFO-Z$_{EGFR:03115}$ administration spiked with different amounts of non-labeled Z$_{EGFR:03115}$ in mice bearing CAL27 tumors: I) 2 µg of $^{89}$Zr-DFO-Z$_{EGFR:03115}$ administered; II) 1 µg of Z$_{EGFR:03115}$ injected 30 mins prior to injection of 2 µg of $^{89}$Zr-DFO-Z$_{EGFR:03115}$; III) 5 µg of Z$_{EGFR:03115}$ injected 30 mins prior to injection of 2 µg of $^{89}$Zr-DFO-Z$_{EGFR:03115}$; IV) 10 µg of Z$_{EGFR:03115}$ injected 30 mins prior to injection of 2 µg of $^{89}$Zr-DFO-Z$_{EGFR:03115}$; V) 10 µg of Z$_{EGFR:03115}$ co-injected with 2 µg of $^{89}$Zr-DFO-Z$_{EGFR:03115}$.

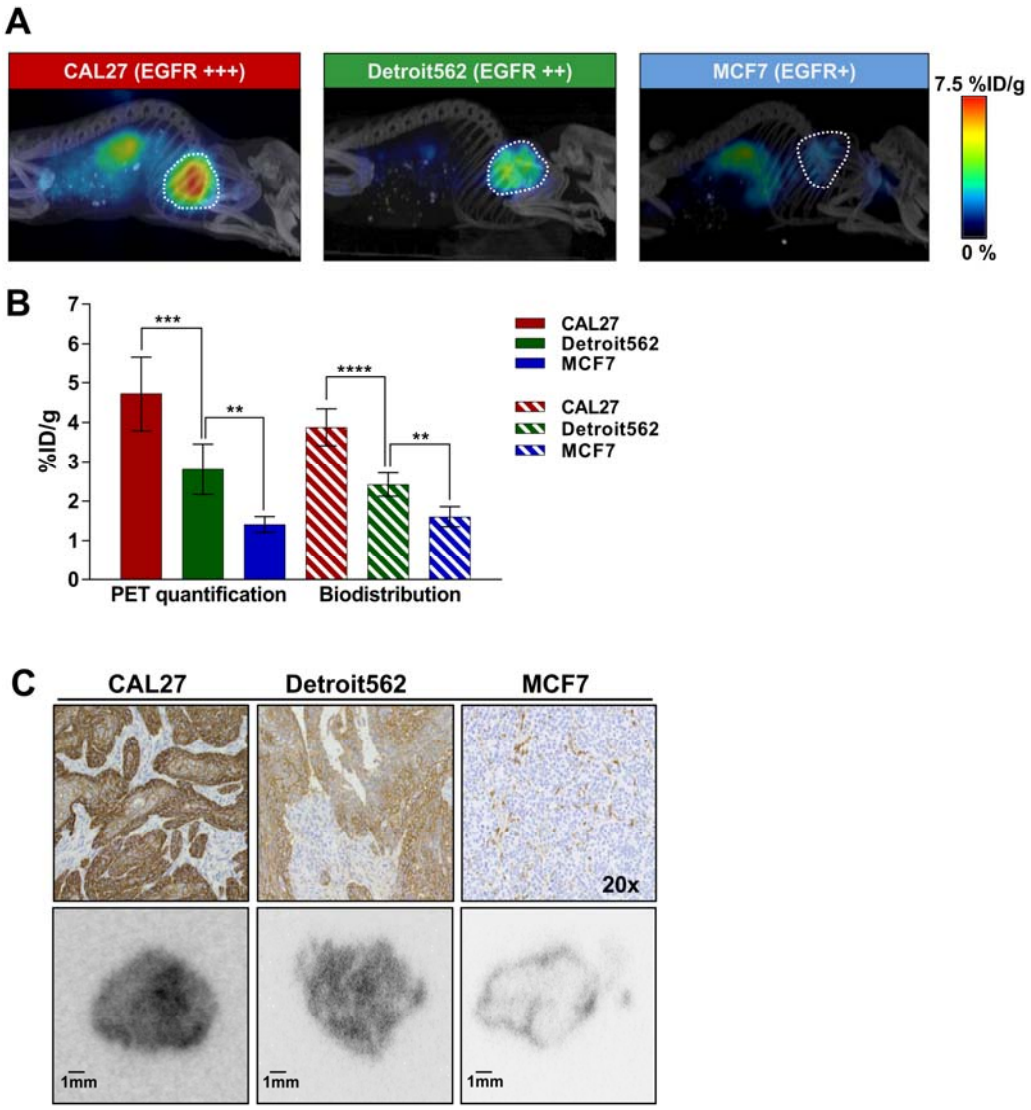


**Figure 4:** Radioconjugate uptake in xenografts with varying EGFR expression. Representative whole-body sagittal fused PET/CT images acquired 3 h after injection (A). PET quantification of radiotracer uptake in tumors (outlined on the image) 3 h after injection in comparison with data obtained from the biodistribution studies. Data are presented as mean ± SD (****$P$ < 0.0001, ***$P$ < 0.001, **$P$ < 0.01) (B). Histopathological analysis of EGFR expression in the xenograft models ($C_{Top}$). Representative autoradiography tumor sections 3 h post radioconjugate administration ($C_{Bottom}$).

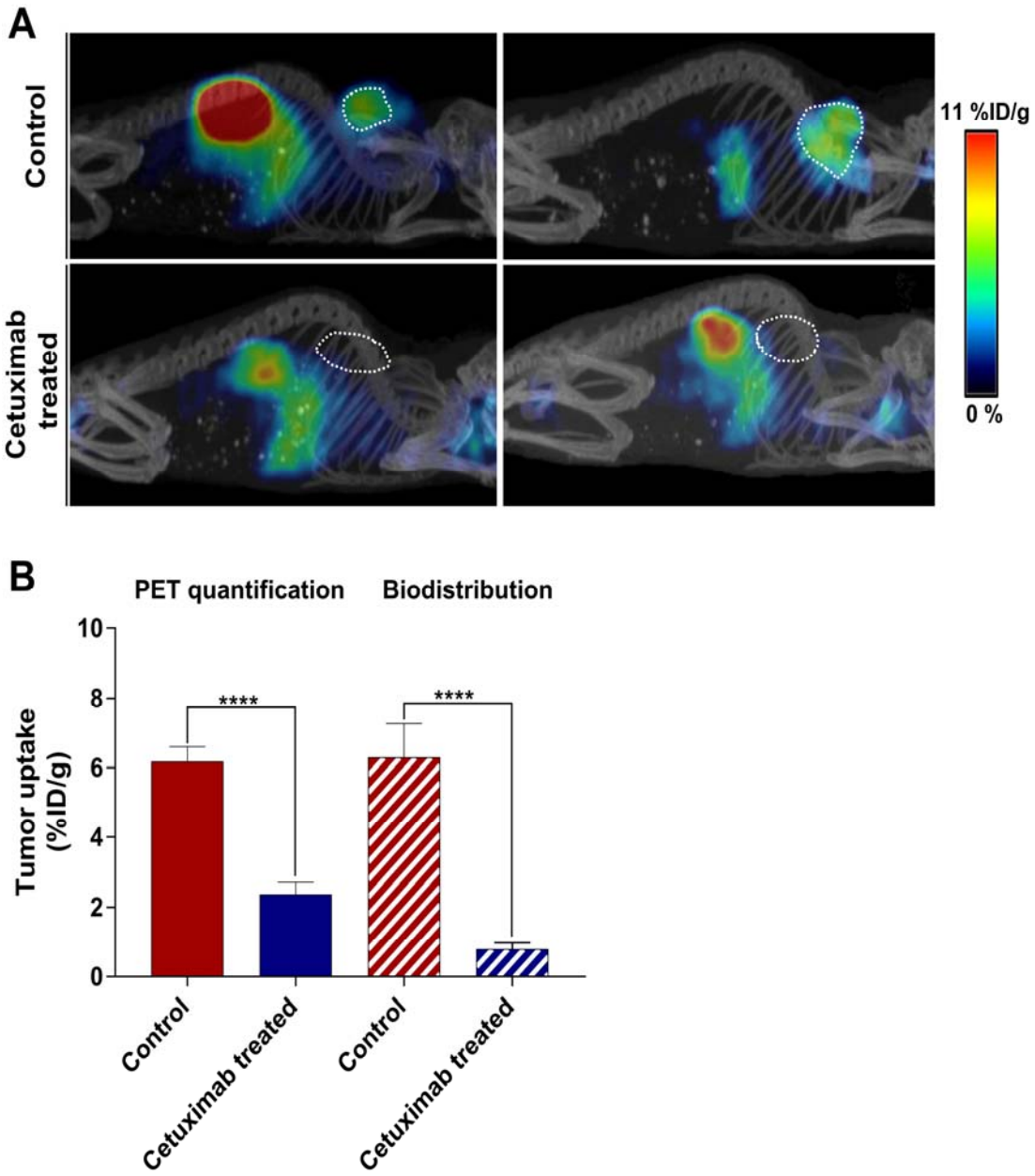


**Figure 5:** $^{18}$F-AlF-NOTA-$Z_{EGFR:03115}$ uptake assessed 1 h post-injection. Representative sagittal whole-body fused PET/CT images of mice bearing HN5 tumors (outlined on the image) with or without treatment with cetuximab (A). PET quantification in control and cetuximab treated HN5 tumors and corresponding biodistribution %ID/g values (B). Data are reported as mean ± SD (n ≥ 6); (****$P$ < 0.0001).

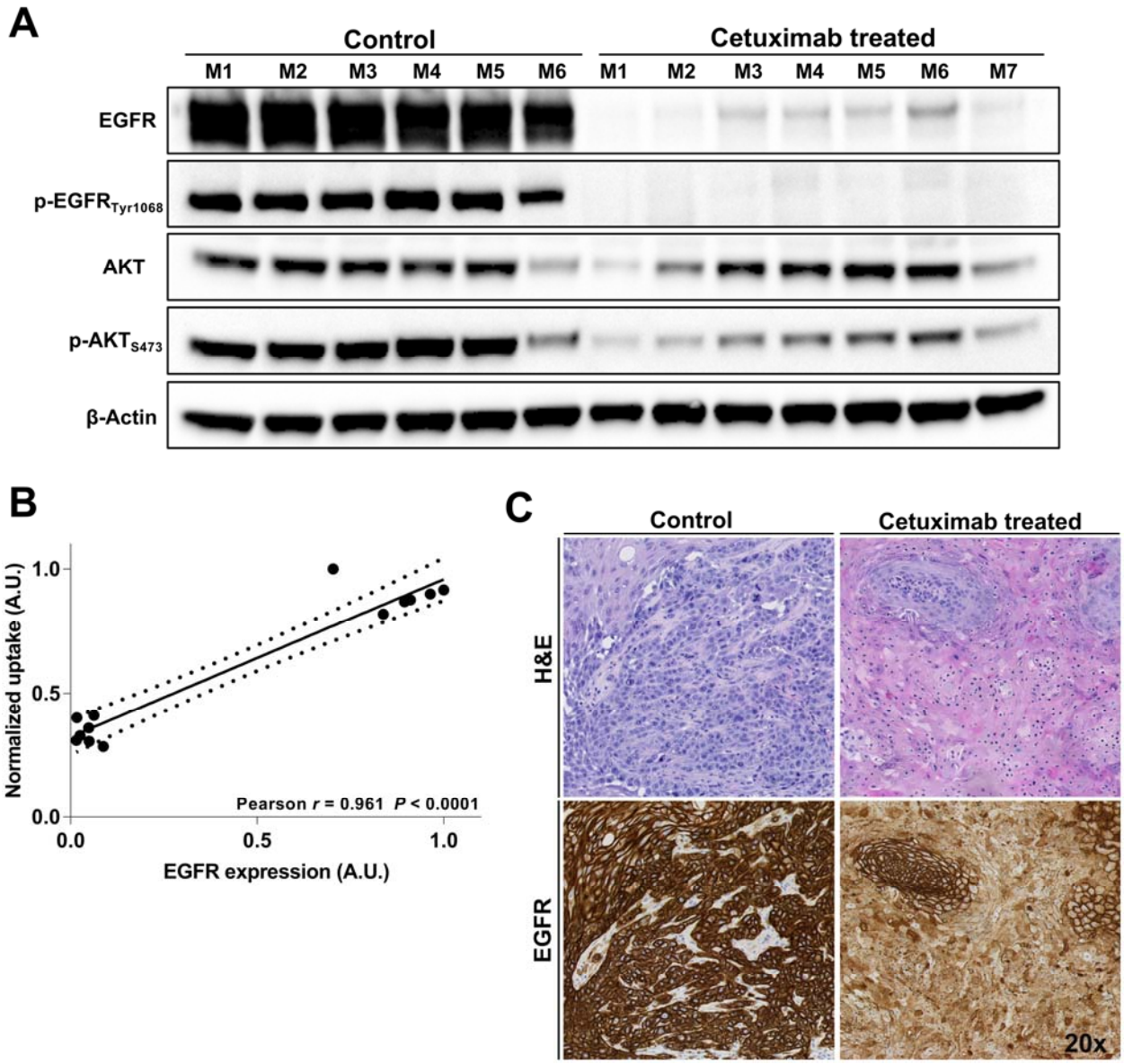


**Figure 6:** Western blot of tumor tissue lysates from control and cetuximab treated mice demonstrating EGFR protein expression, activation and downstream signaling (A). Spearman's rank correlation analysis for EGFR expression as determined by Western blot against $^{18}$F-AlF-NOTA-Z$_{EGFR:03115}$ tumor uptake as quantified by PET image analysis. The dashed lines represent the 95% confidence levels (B). Histopathological analysis of EGFR expression and H&E staining in HN5 xenografts in both a control and cetuximab treated mouse (C).

| Organ (%ID/g) | 2 μg $^{89}$Zr-DFO-$Z_{EGFR:03115}$ | | | | | 2μg $^{89}$Zr-DFO-$Z_{Taq}$ |
|---|---|---|---|---|---|---|
| | 0 μg $Z_{EGFR:03115}$ | 1 μg $Z_{EGFR:03115}$ | 5 μg $Z_{EGFR:03115}$ | 10 μg $Z_{EGFR:03115}$ | 20 μg $Z_{EGFR:03115}$ | 10μg $Z_{EGFR:03115}$ |
| **Blood** | 3.52±1.42 | 6.01±0.18 | 3.87±0.30 | 4.46±1.65 | 3.06±0.20 | 0.64±0.04 |
| **Heart** | 0.89±0.22 | 1.53±0.05 | 0.95±0.09 | 1.03±0.29 | 0.77±0.06 | 0.25±0.03 |
| **Lungs** | 1.45±0.45 | 2.55±0.23 | 1.84±0.50 | 2.05±0.1.06 | 1.45±0.08 | 0.47±0.05 |
| **Kidney** | 37.14±1.17 | 54.52±17.13 | 73.26±12.91 | 140.84±47.70 | 109.14±22.30 | 172.04±20.07 |
| **Spleen** | 0.91±0.10 | 1.58±0.23 | 0.94±0.20 | 1.28±0.13 | 0.94±0.13 | 0.37±0.08 |
| **Liver** | 20.74±8.31 | 10.36±1.49 | 3.82±0.39 | 4.25±1.55 | 3.19±0.14 | 0.82±0.22 |
| **Pancreas** | 0.73±0.19 | 1.62±0.24 | 0.71±0.12 | 0.69±0.13 | 0.46±0.04 | 0.14±0.03 |
| **Tumor** | 1.75±0.21 | 1.70±0.68 | 1.87±0.58 | 3.69±1.19 | 2.59±0.48 | 0.26±0.05 |
| **Bone** | 1.35±0.24 | 1.24±0.21 | 0.81±0.15 | 0.87±0.14 | 0.66±0.09 | 0.21±0.05 |
| **Intestine** | 0.59±0.28 | 1.62±0.57 | 0.90±0.11 | 0.89±0.11 | 0.81±0.05 | 0.19±0.03 |
| **Muscle** | 0.24±0.01 | 0.35±0.07 | 0.37±0.09 | 0.36±0.05 | 0.33±0.04 | 0.08±0.03 |
| **Tumor/Blood** | **0.50** | **0.28** | **0.48** | **0.83** | **0.85** | **0.41** |
| **Tumor/Muscle** | **7.29** | **4.86** | **5.05** | **10.25** | **7.85** | **3.15** |
| **Tumor/Liver** | **0.08** | **0.16** | **0.49** | **0.87** | **0.81** | **0.32** |

**Table 1:** Biodistribution results 3 h post-administration of increasing amounts of non-labeled $Z_{EGFR:03115}$ 30 mins prior to 2 μg $^{89}$Zr-DFO-$Z_{EGFR:03115}$ or 2 μg $^{89}$Zr-DFO-$Z_{Taq}$ in CAL27 xenografts. Data are reported as mean ± SD (n ≥ 3) of injected dose per gram of tissue.

| Organ (%ID/g) | 3 h | 24 h | 48 h |
|---|---|---|---|
| **Blood** | 3.70±0.55 | 0.87±0.32 | 0.23±0.06 |
| **Heart** | 0.99±0.19 | 0.37±0.12 | 0.31±0.04 |
| **Lungs** | 2.74±0.93 | 0.88±0.13 | 0.70±0.08 |
| **Kidney** | 130.42±22.25 | 108.80±19.60 | 104.85±11.10 |
| **Spleen** | 1.14±0.18 | 0.72±0.20 | 0.79±0.37 |
| **Liver** | 4.99±0.85 | 4.31±1.00 | 4.11±1.41 |
| **Pancreas** | 0.67±0.14 | 0.36±0.10 | 0.35±0.25 |
| **Tumor** | 3.88±0.46 | 2.43±0.27 | 2.13±0.12 |
| **Bone** | 0.99±0.28 | 2.28±0.27 | 3.44±0.59 |
| **Intestine** | 1.09±0.16 | 0.42±0.03 | 0.40±0.02 |
| **Muscle** | 0.38±0.09 | 0.14±0.04 | 0.16±0.07 |
| **Tumor/Blood** | **1.04** | **2.79** | **9.34** |
| **Tumor/Muscle** | **10.31** | **17.35** | **13.56** |
| **Tumor/Liver** | **0.78** | **0.56** | **0.52** |

**Table 2:** *Ex vivo* biodistribution results 3, 24 and 48 h post $^{89}$Zr-DFO-$Z_{EGFR:03115}$ injection. Data are reported as mean ± SD (n ≥ 3) of injected dose per gram of tissue following the intravenous injection of 2 µg $^{89}$Zr-DFO-$Z_{EGFR:03115}$ co-injected with 10 µg non-labeled $Z_{EGFR:03115}$ in mice bearing CAL27 xenografts.

The Journal of NUCLEAR MEDICINE

# Affibody-based PET imaging to guide EGFR-targeted cancer therapy in head and neck squamous cell cancer models

Thomas A. Burley, Chiara Da Pieve, Carlos D. Martins, Daniela M. Ciobota, Louis Allott, Wim J. G. Oyen, Kevin J. Harrington, Graham Smith and Gabriela Kramer-Marek

*J Nucl Med.*
Published online: September 13, 2018.
Doi: 10.2967/jnumed.118.216069



*The Journal of Nuclear Medicine* is published monthly.
SNMMI | Society of Nuclear Medicine and Molecular Imaging
1850 Samuel Morse Drive, Reston, VA 20190.
(Print ISSN: 0161-5505, Online ISSN: 2159-662X)



SNMMI SOCIETY OF NUCLEAR MEDICINE AND MOLECULAR IMAGING